Effect of Short-Chain Branching on Melt Fracture Behavior of Metallocene and Conventional Poly(Ethylene/α-Olefin) Copolymers

E. Garofalo, L. Incarnato, L. Di Maio
Department of Industrial Engineering, University of Salerno, Fisciano (SA) 84084 Italy

A phenomenon that can represent a great problem in melt processing is extrudate distortion. This effect can range in intensity from a loss of gloss to gross distortion and is the factor that limits the production rate in certain processes such as the blown film extrusion of linear low-density polyethylene (LLDPE). The aim of this work was to investigate the effects that molecular weight distribution and short-chain branch length have on the observed melt fracture phenomena for poly(ethylene/α-olefin) resins with similar weight comonomer content and molecular weight. The flow stability analysis conducted in this study has shown that, even increasing of few carbon atoms the short-chain branch length of the resins, the surface melt fracture phenomena are reduced and/or eliminated. Moreover, the comparison between the metallocene (mLLDPE) and conventional LLDPE samples, with the same comonomer (hexene), showed that the metallocene-catalyzed resin exhibits early onset and more severe melt fracture, due to its narrower molecular weight distribution. POLYM. ENG. SCI., 00:000–000, 2012. © 2012 Society of Plastics Engineers

INTRODUCTION

In many extrusion processes (e.g. cast and blown film extrusion, wire coating, etc.), the rates of industrial production are often limited by the onset of flow instabilities that perturb the profile of the extrudate. Such problem arises when a molten polymer is extruded through a die at a throughput exceeding a critical value and the phenomenon of melt fracture occurs. Because of these instabilities, in worst cases, the material surface could result rough and the final products become commercially unacceptable.

The melt fracture evolves through different types of instabilities as the flow rate in the die is increased. In particular, it can range from a simple loss of surface gloss to the so-called gross fracture, which involves a severe extrudate distortion. In the literature, melt fracture is usually classified into three separate types: surface melt fracture (SMF) also called sharkskin, slip-stick fracture (SSF), and gross melt fracture (GMF) [1, 2].

Since the SMF occurs early above the critical flow conditions, it is mostly studied and there is a general agreement that the initiation of sharkskin is located at the die exit [3, 4]. In particular, Howells [3] and Cogswell [4] hypothesized that polymer fracture at the die exit is due to high extensional stresses that develop at this location. The melt leaving the die in the neighborhood of the wall experiences a large, rapid, tensile deformation as the velocity field adjusts from the no-slip boundary condition to the free-surface condition, causing the propagation of surface cracks, responsible for the sharkskin topography. Another well-known mechanism leading to the sharkskin is the slippage (adhesive failure) between the polymer melt and the die wall [5–7]. When the debonding stress between the wall and the polymer melt is less than the cohesive strength of the melt resin, the polymer slips on the wall at levels of the wall shear stress higher than the debonding stress. If the slip does not take place constantly, it will lead to surface instabilities such as stick-slip failure, observed with increasing the shear rate. Furthermore, Brochard and de Gennes [8] proposed another molecular theory, in which disentanglements between bulk polymer chains and the polymer chains adhered on the wall (cohesive failure) are the origin of surface instabilities (SMF and SSF). Finally, at the highest flow rates, GMF takes place and it is characterized by a highly irregular extrudate. The GMF is generally associated to the high elongation stresses due to the contraction of the flow in the entry of the die [9, 10].

It is well known that the type and severity of melt fracture depend on the molecular structure of the extruded material. In particular, linear polyethylenes (high-density polyethylene) can exhibit all of three types of melt fracture [6, 11]. In opposition, long-branched polyethylenes (low-density polyethylene) do not show any of all the three types of melt fracture, but shift from smooth

Correspondence to: E. Garofalo; e-mail: egarofal@unisa.it
Contract grant sponsor: POR Campania 2000/2006 and by European Community "Programma Operativo 2007-2013, Obiettivo operativo 2.2, attività a) Utilizzo di specifiche formulazioni di Polietilene in sostituzione del Polipropilene per la realizzazione di film plastici destinati alla realizzazione di packaging alimentare."
DOI 10.1002/pen.23140
Published online in Wiley Online Library (wileyonlinelibrary.com).

TABLE 1. Characteristics of the materials studied.

Resin	Density (g/cm^3)	Molar comonomer content (mol%)	Weight comonomer content (wt%)	η_0 (Pa s)	M_w (g/mol)	E_a (kJ/mol)
LLDPE/butene	0.918	4.2	8.1	3300	99,000	29
LLDPE/hexene	0.920	3.9	10.1	3000	97,000	28
mLLDPE/hexene	0.918	3.2	9.0	1900	85,000	31
LLDPE/octene	0.917	2.6	9.6	2650	94,000	29

extrudate directly to a grossly deformed one above an apparent critical wall shear stress of the order of 10^5 Pa [12, 1]. The influence of branching on the properties and processability of polyethylenes has gained great interest during the last years. In particular, a controlled amount of short-chain branches can be incorporated by polymerizing ethylene with a comonomer, such as an α-olefin, in order to improve the performances of the resins [13, 14]. Moreover, recent development of metallocene catalyst technology makes it possible to produce a tailored ethylene/α-olefin copolymer at a commercial scale. Since metallocene polymers have a narrower molecular weight distribution (MWD) compared with conventional polyolefins obtained by Ziegler-Natta catalyst, flow instabilities often take place early and limit the production speed [15–17].

The effects of various molecular parameters, such as molecular weight, polydispersity, and long-chain branching, on flow instabilities of polyethylenes have been deeply studied, while the influence of the different of α-olefin units (butene, hexene, octene, etc.) and their distribution along the chains of linear low-density polyethylene (LLDPE) copolymers has not been extensively investigated. In this study, the molecular characteristics and processing behavior of a set of conventional and metallocene polyethylene copolymers have been correlated. In particular, the aim of this work was to investigate the effects that MWD and short-chain branch (SCB) length have on the observed melt fracture phenomena for LLDPE/α-olefin resins with similar weight comonomer content and molecular weight. Furthermore, the effect of temperature on melt fracture behavior has also been analyzed. For these purposes, rheological measurements were performed in both shear and extensional flow, and melt extrusion experiments were carried out at different temperatures using a rate controlled capillary rheometer.

EXPERIMENTAL

Materials

Four commercial LLDPEs were employed for this study: three conventional LLDPE/α-olefin copolymers (Flexirene CL10U, Clearflex CL106, Dowlex SC2107) and a metallocene LLDPE/α-hexene (Exceed m3518CB). The weight content of comonomer was similar in all the resins investigated. The relevant physical and molecular characteristics of these materials are summarized in Table 1. For the calculation of the weight comonomer content w_c from the molar comonomer content n_c, the relation $w_c = n_c \times l/[n_c \times (l - 2) + 2]$ was used, where l is the length of the comonomer in numbers of carbon atoms [18].

Characterization

Rheological measurements in oscillatory mode were performed at different temperatures (190, 200, 210, and 220°C) with a Rheometric Scientific rotational rheometer (ARES) in an angular frequency range from 0.1 to 100 rad/s and using 25-mm diameter parallel plates. The deformation of 5% of strain amplitude was proven to ensure linear viscoelasticity of the dynamic tests. Time-temperature superposition was applied to obtain the master linear viscoelastic curves at the reference temperature of 220°C.

Transient elongational data were obtained using a new extensional rheology test fixture, the Sentmanat Extensional Rheometer (SER) [19, 20]. This instrument (model SER-HV-A01, manufactured by Xpansion Instruments) was designed for use as a detachable tool on ARES. Samples for testing were prepared by compression moulding, using a preheated hydraulic press, and cut into small rectangles with the following dimensions: thickness, width and length of 0.8 mm × 6 mm × 15 mm, respectively, which were specifically chosen within the recommended ranges of sample dimensions for optimum instrument performance [19]. The elongational tests were carried out at 150°C and at a Hencky strain rate of 20 s^{-1}, until the maximum achievable Hencky strain (equal to 3.8).

Capillary extrusion experiments were performed at various temperatures (150, 190, 200, 210, and 220°C) by means of a capillary rheometer (Rosand RH7, Bohlin Instruments) equipped with a capillary die made of tungsten carbide and having a diameter of 1 mm (L/D = 15) and an entrance angle of 180°. Polymer samples, extruded under steady state conditions, were collected and then inspected by means of an optical microscope to detect the presence and type of melt fracture.

RESULTS AND DISCUSSION

Rheological Characterization at Low-Shear Rates

Oscillatory shear mode tests, within the linear viscoelastic range, were performed on four commercial LLDPE copolymers in order to obtain useful information about the molecular structure of these materials. Figure 1 shows

 DOI 10.1002/pen

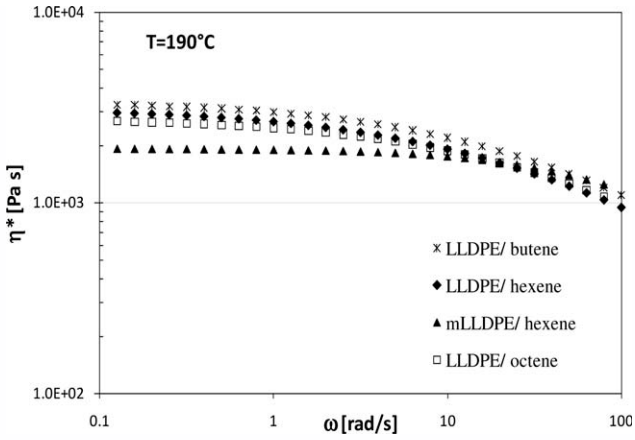

FIG. 1. Complex viscosity curves of conventional LLDPEs and mLLDPE at 190°C.

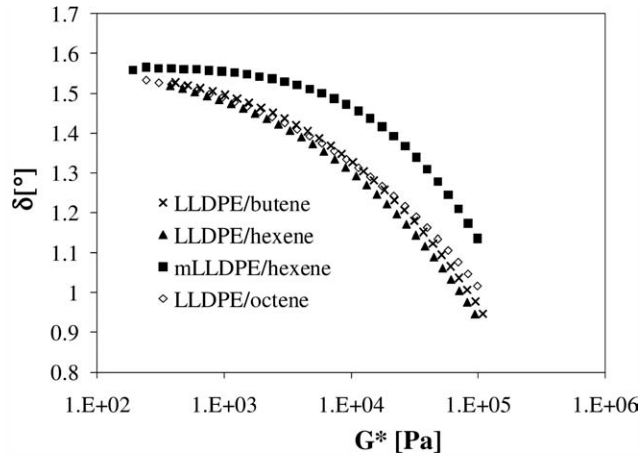

FIG. 3. Van Gurp plots of conventional LLDPEs and mLLDPE at 190°C.

the complex viscosity plots at 190°C for all the resins studied. It can be seen that the conventional LLDPEs exhibit similar rheological behavior. In particular, compared with the metallocene resin, they show higher complex viscosity values at low frequencies and a more pronounced shear thinning behavior at high frequencies. The zero-shear viscosity values were obtained by the experimental rheological data in order to calculate the molecular weight (M_w) of the resins by means of the following relationship:

$$\eta_0 = 3.4 \times 10^{-15} \cdot M_W^{3.6} \quad (1)$$

valid for linear polyethelenes at 190°C. [21]. This equation is independent of MWD [22–24] and can be applied to LLDPE samples with small short-chain branching degree [22, 25]. In Table 1 the zero-shear viscosity values and M_w of all the samples at 190°C are summarized.

The shear flow curves of entangled polymers are influenced by the M_w, its distribution, and the level of long-chain branching (LCB) in a convoluted manner [26]. In particular, since polydispersity and LCB affect the shear rheological behavior in the same way, several authors have proposed correlations in order to assess independently the effect of these two molecular features on the rheological properties of the resins [27]. It is worth to point out that even small amount of LCB in metallocene polyethylene significantly influences the properties of the polymer [28] and, recently, there is a considerable interest in detecting sparse LCB (<1 branch per chain) in LLDPE by rheological tests [27]. Mavridis and Shroff [29] have shown that in the case of linear polyethylenes (high density and linear low density) the viscoelastic moduli data, reported in a Cole-Cole plot (G″ versus G′) and measured at different temperatures, lie on a single master curve, regardless of resin polydispersity. On the other hand, in presence of LCB a vertical shift of the data is necessary to obtain a single master curve when the time-temperature superposition is applied. At this regard, Cole-Cole plots for all the samples analyzed in this work were obtained at different temperatures (190, 200, 210, and 220°C), but for clarity in Fig. 2 the curves for LLDPE/hexene and mLLDPE/hexene resins are reported only. All the visco-

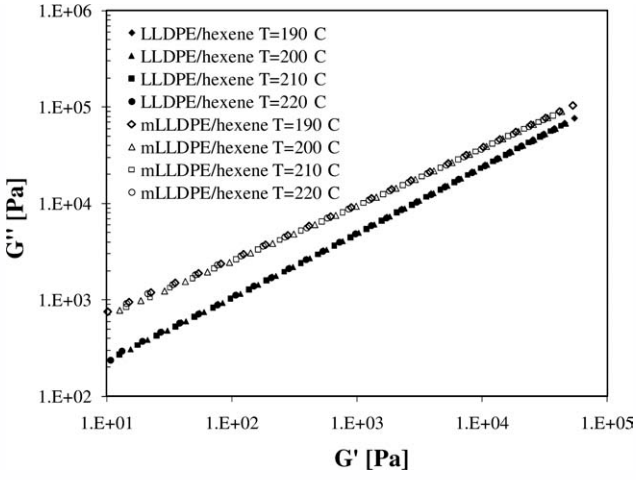

FIG. 2. Cole-Cole plots of LLDPE/hexene and mLLDPE/hexene resins, reporting the viscoelastic moduli data obtained at different temperatures.

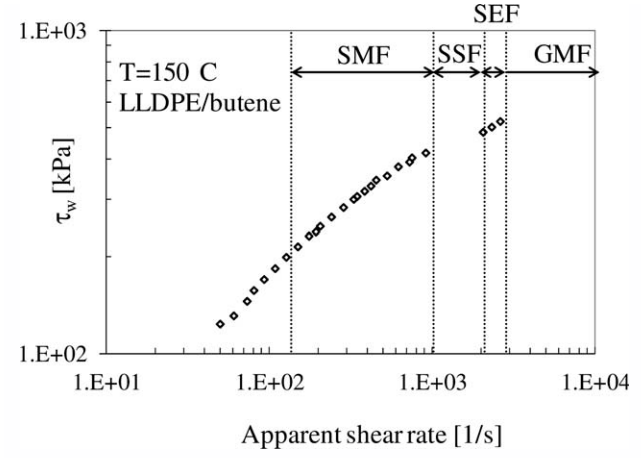

FIG. 4. Flow curve of LLDPE/butene at 150°C: SMF = surface fracture region, SSF = stick-slip fracture region, SEF = superextrusion flow, GMF = gross melt fracture region.

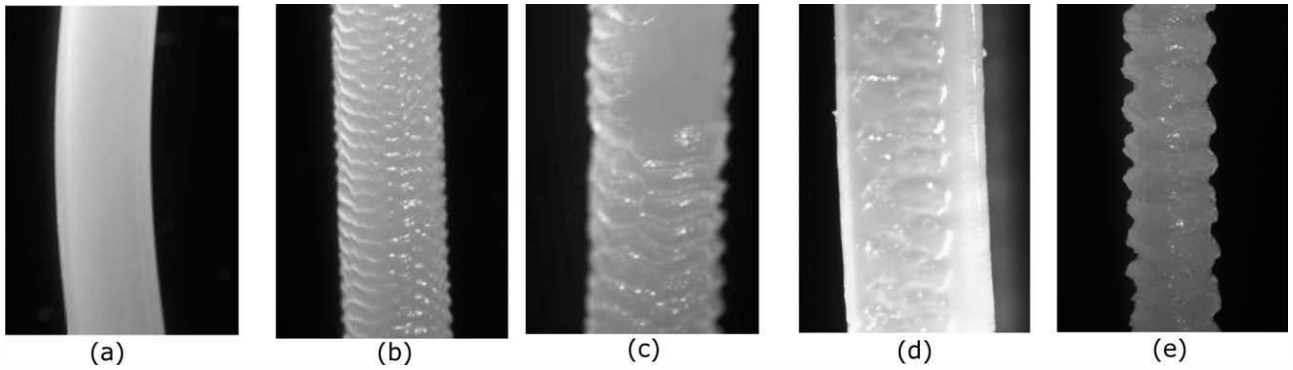

FIG. 5. Images of LLDPE/butene extrudates at apparent shear rates of: (a) 100 s^{-1}; (b) 300 s^{-1}; (c) 920 s^{-1}; (d) 2000 s^{-1}; (e) 2600 s^{-1}.

elastic moduli data lie on a single master curve for each sample, showing that none of the studied LLDPE copolymers has sparse long-chain branching. In order to exhibit more clearly the effect of polydispersity on the rheological properties of the resins, the Van Gurp plots at 190°C are also reported (Fig. 3). It can be seen that all the conventional LLDPEs show a similar trend and lower values of the phase angle δ compared with the metallocene resin. From these results, it can be deduced that the Ziegler-Natta catalyzed samples have MWD similar between them and a broader polydispersity respect to the mLLDPE.

Based on the rheological characterization at low deformation rates in shear mode, it can be concluded that the LLDPEs analyzed do not possess sparse LCB and have similar molecular weight. The conventional LLDPEs also exhibit similar MWD and differ only for the comonomer type. Comparing the resins with the same comonomer (hexene), the metallocene polyethylene has narrower MWD respect to the corresponding Ziegler-Natta catalyzed LLDPE.

Melt fracture phenomena are also strongly influenced by the extrusion temperature. At this regard the flow activation energy E_a represents a useful parameter to measure the temperature sensitivity of the resins. Since the rheological properties of all LLDPE samples analyzed in this work obey the time-temperature superposition principle, the Arrhenius relation (Eq. *2*) can be applied, at temperatures well above the glass transition temperature of the polymers, in order to calculate the flow activation energy E_a:

$$a_{\mathrm{T}} = \frac{\eta_0(T)}{\eta_0(T_0)} = \exp\left[\frac{E_{\mathrm{a}}}{R}\left(\frac{1}{T} - \frac{1}{T_0}\right)\right] \tag{2}$$

where T_0 is the reference temperature (taken equal to 220°C here). The values of the calculated activation energy, E_a, are reported in Table 1. The activation energies of conventional LLDPEs were found to be quite similar for each sample and to be around 28–29 KJ/mol, while a slightly higher value (31 KJ/mol) was reported for the metallocene-catalyzed linear low density polyethylene, in agreement with the data earlier reported in literature [18, 30].

Capillary Extrusion Experiments

Capillary extrusion experiments at high shear rates were performed in order to study the evolution of melt fracture behavior for the selected LLDPE copolymers. In particular, the flow curves in terms of the apparent shear stress (τ_w) as function of the apparent wall shear rate ($\dot{\gamma}_{\mathrm{a}}$) were obtained at different temperatures.

The flow curve for LLDPE/butene sample at a temperature of 150°C is plotted in Fig. 4, where the characteristic flow regimes of the resin have also been evidenced. Moreover, the images in Fig. 5 clearly illustrate the evolution of melt fracture behavior in this polyethylene copolymer. In particular, sharkskin is first observed at $\dot{\gamma}_{\mathrm{a}} = 130s^{-1}$ ($\tau_w = 0.20$ MPa), corresponding to a slight matting of the extrudate surface. Higher flow rates led to noticeable increases in the severity of SMF as evidenced by micrograph obtained at $\dot{\gamma}_{\mathrm{a}} = 300s^{-1}$. Beyond $\dot{\gamma}_{\mathrm{a}} = 920s^{-1}$ the flow becomes unstable, being a phenomenon associated with the onset of stick-slip fracture that corresponds to a critical wall shear stress of 0.42 MPa and a range of apparent shear rates. This instability splits the flow curves into two branches [11]. In particular, it can be noted that for LLDPE/butene resin the onset of GMF ($\dot{\gamma}_{\mathrm{a}} = 2600s^{-1}$) does not coincide with the beginning of the high flow rate

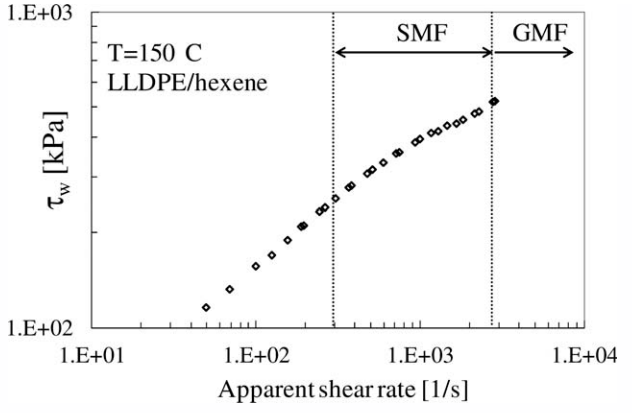

FIG. 6. Flow curve of LLDPE/hexene at 150°C: SMF = surface fracture region, GMF = gross melt fracture region.

 DOI 10.1002/pen

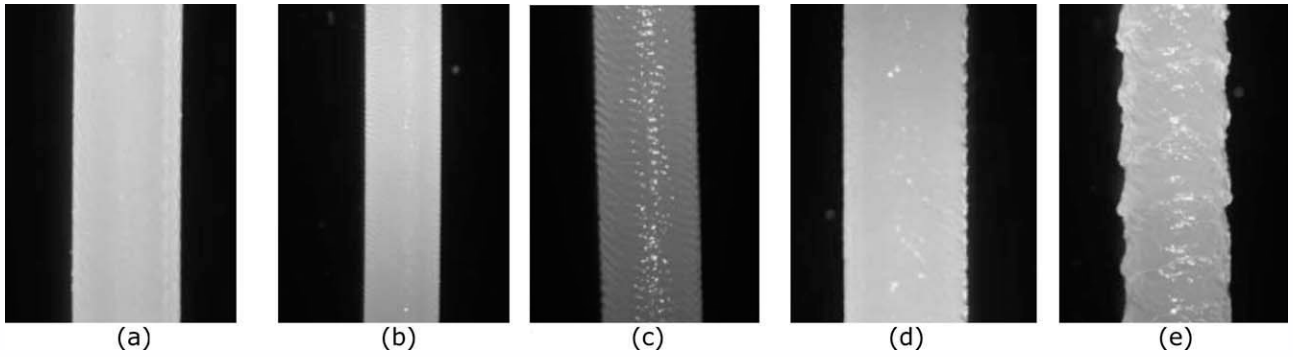

FIG. 7. Images of LLDPE/hexene extrudates at apparent shear rates of: (a) 125 s^{-1}; (b) 250 s^{-1}; (c) 600 s^{-1}; (d) 1200 s^{-1}; (e) 2800 s^{-1}.

branch. A superextrusion flow [31] can be identified at apparent shear rates greater than about 2000 s^{-1}, where the extrudate appears relatively smooth.

The flow curve of LLDPE/hexene resin at 150°C is presented in Fig. 6. The stable flow region extends to higher shear rates and the onset of SMF is delayed until $\dot{\gamma}_a = 250s^{-1}$, which corresponds to an apparent wall shear stress of 0.23 MPa. The images, presented in Fig. 7, clearly show that increasing the flow rate also increases the severity of SMF. Over the shear rate of 600 s^{-1} the surface irregularities gradually transform from sharkskin to screw thread-like distortions and a further increase of shear rate (1200 s^{-1}) leads to relatively smooth extrudate surfaces. Most surprisingly, no clear evidence of stick-slip fracture was observed for the LLDPE/hexene resin, even if the inflection point in the flow curve at 1800 s^{-1} may indicate possible stick-slip fracture behavior. Assuming that no slip-stick region is present, or that its range is very narrow, the next melt fracture regime observed was GMF at $\dot{\gamma}_a = 2800s^{-1}$ and at a critical wall shear stress of 0.52 MPa, corresponding to significant extrudate distortions.

The linear metallocene ethylene copolymer (mLLDPE/hexene) shows an early onset of SMF ($\dot{\gamma}_a = 190s^{-1}$ and $\tau_w = 0.30$ MPa) compared with the conventional LLDPE/hexene resin, as evidenced by both the flow curve and the extrudate images reported in Figs. 8 and 9 respectively. Further increments in flow rates lead to dramatic increases in the severity of SMF. Moreover, contrary to the corresponding Ziegler-Natta polyethylene, mLLDPE/hexene also exhibits SSF in the range of shear rates 500–1700 s^{-1}, corresponding to a critical wall shear stress of 0.44 MPa. The GMF regime is then observed at $\dot{\gamma}_a = 1700s^{-1}$.

The flow curve obtained for the LLDPE/octene sample is plotted in Fig. 10 and the images of the corresponding extrudates are reported in Fig. 11. As evidenced by both the flow curve and the images of the capillary die extrudates, this resin shows three distinct flow regimes. The first region represents stable flow and smooth extrudates are obtained until critical shear rates of 500 s^{-1} ($\tau_w = 0.24$ MPa). Beyond these flow conditions, it is observed that SMF gradually varies from sharkskin to screw thread-like distortions by increasing the shear rate. The GMF regime is then observed at $\dot{\gamma}_a = 2800s^{-1}(\tau_w = 0.55$ MPa), while no evidence of stick-slip fracture appears for the conventional LLDPE/octene resin.

The values of critical shear rates and stresses in capillary die extrusion at 150°C for all the resins investigated are summarized in Table 2. The capillary extrusion experiments conducted on the Ziegler-Natta LLDPEs indicate that they show SMF at shear stress in the range 0.20–0.34 MPa (Table 2). The critical wall shear rate for the onset of sharkskin of the conventional LLDPE copolymers was found to vary between 130 and 500 s^{-1}. In particular, the Ziegler-Natta linear polyethylenes studied in this work exhibit a delayed onset of SMF with increasing the SCB length and it is interesting to note that the critical shear rate, corresponding to sharkskin phenomenon, increases about twice by progressively increasing the comonomer length of two carbon atoms (Table 2). Indeed, the sample LLDPE/octene can be processed at the highest shear rate ($\dot{\gamma}_a = 500s^{-1}$), compared with the other conventional LLDPE copolymers, without exhibiting any flow instabilities.

There is a general agreement that the site of initiation of sharkskin is located at the die exit, where high exten-

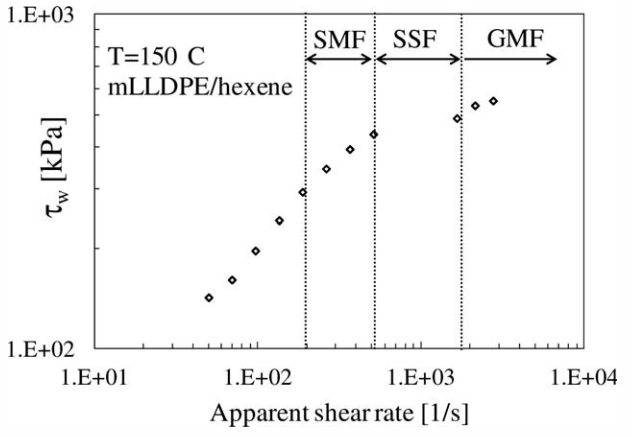

FIG. 8. Flow curve of mLLDPE/hexene at 150°C: SMF = surface fracture region, SSF = stick-slip fracture region, GMF = gross melt fracture region.

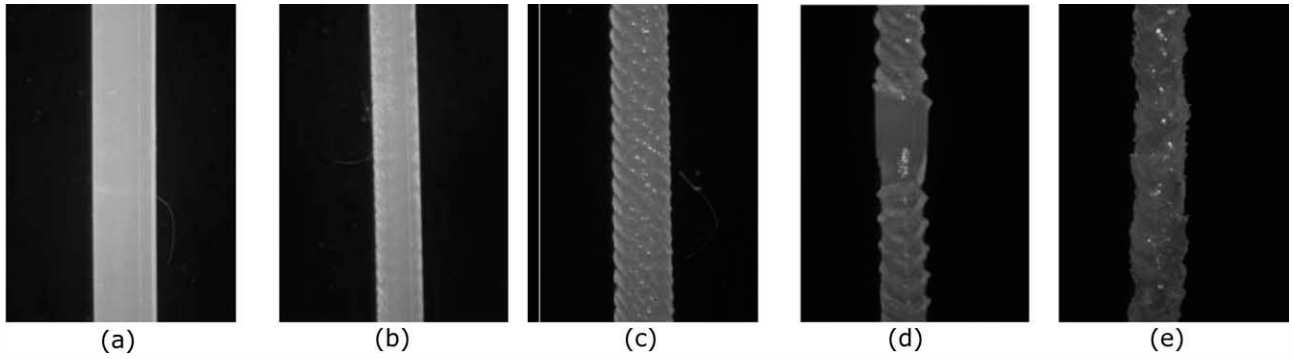

FIG. 9. Images of mLLDPE/hexene extrudates at apparent shear rates of: (a) 140 s^{-1}; (b) 190 s^{-1}; (c) 270 s^{-1}; (d) 500 s^{-1}; (e) 1700 s^{-1}.

sional stresses develop. The periodicity of the sharkskin melt fracture occurs as a result of the intermittent elastic energy storage and elastic energy dissipation along the surface of the extrudate. Consequently, linear polyethylenes are inclined to this type of melt fracture phenomenon since, at high extensional flow rates, they exhibit both a rapid increase in elastic tensile modulus and a brittle-type mode of failure, factors that inherently contribute to crack propagation [32, 11].

In this work, the relation between the SMF phenomenon and the high-extensional flow behavior of the polymer melts was studied. The plots of tensile stress (σ_E) as function of Hencky strain (ε_H) for LLDPE/butene, LLDPE/hexene and mLLDPE/hexene samples are reported in Fig. 12 at a Hencky strain rate of 20 s^{-1} and at temperature of 150°C. The stress-strain curve for the copolymer LLDPE/octene was not plotted in Fig. 12, because this resin shows an onset of sharkskin at relatively higher critical shear rate (Table 2), compared with the other polyethylenes studied in this paper and respect to other LLDPE resins analyzed in literature [11]. As consequence, the extensional rate, relevant to the occurrence of sharkskin for the LLDPE/octene copolymer, results higher than 20 s^{-1} that approaches the upper value of Hencky strain rate achievable with SER on our rotational rheometer, due to limitations with the transducer compliance.

It is evident from the curves in Fig. 12 that LLDPE/butene and mLLDPE/hexene samples exhibit a more rapid increase of the extensional stress compared with the LLDPE/hexene copolymer. This latter resin dissipates better the elastic energy associated with the rapid extensional deformation on the surface of the extrudate upon exiting the die, delaying the onset of the SMF (Table 2). Therefore, a correlation between the critical shear rate for the onset of sharkskin and the tensile elastic modulus exists for conventional LLDPE/α-olefin copolymers differing only for the length of the short-chain branches. These experimental results agree well with the trend observed by other authors that correlate the onset of flow instabilities with the high-rate extensional behavior of linear and long-branched polyethylenes [32]. Moreover, the flow stability study conducted in this work confirms that an analysis of the high-rate extensional flow behavior of poly ethylene resins, exhibiting very similar shear flow behavior (Fig. 1), provides fundamental insight into their processability as regarding the occurrence of SMF phenomena [11].

In presence of the same comonomer type (hexene), the metallocene LLDPE shows different extensional rheological properties at high deformation rates, compared with its conventional counterpart (Fig. 12). This can be reasonably attributed to a narrower MWD that affects the earlier onset of SMF of the mLLDPE sample (Table 2).

Kausch [33] further supported the crack mechanism, originally proposed by Cogswell [4], as the main cause of sharkskin instability. They affirm that localized de-cohesion of molecular coils, which takes place in the region with less degree of entanglement couplings, is the primary step of micro-voids leading to macroscopic cracks. As a result, cracks are easily generated in polymers with less entanglement density. In a recent study Yamaguchi et al. [16] found that the onset stress of sharkskin failure for ethylene/α-hexene copolymer decreases rapidly with increasing α-hexene content, since the entanglement density of the resin is reduced.

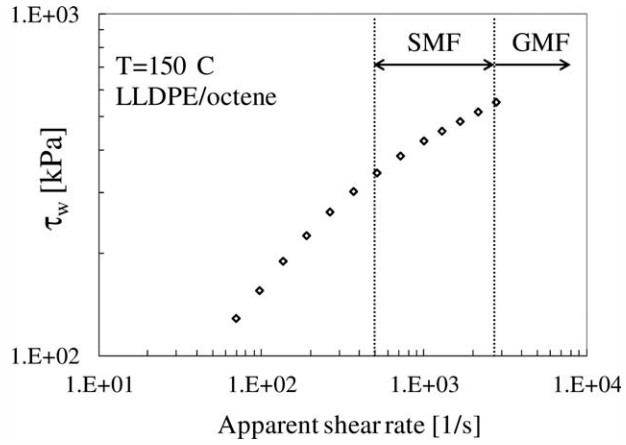

FIG. 10. Flow curve of LLDPE/octene at 150°C: SMF = surface fracture region, GMF = gross melt fracture region.

 DOI 10.1002/pen

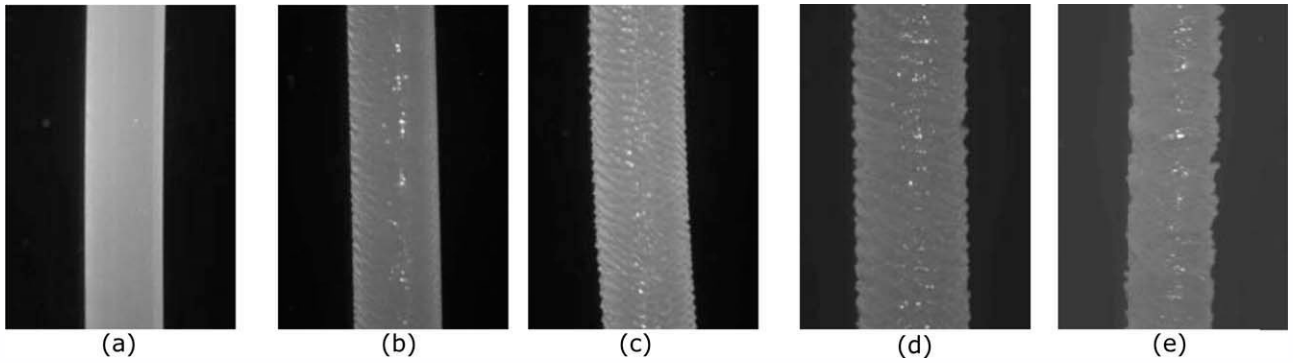

FIG. 11. Images of LLDPE/octene extrudates at apparent shear rates of: (a) 370 s^{-1}; (b) 500 s^{-1}; (c) 720 s^{-1}; (d) 1700 s^{-1}; (e) 2800 s^{-1}.

The conventional LLDPE copolymers analyzed in this work, differing only for the type of the α-olefin used in polymerization, showed an increase in the value of the onset of sharkskin with increasing the length of the short-chain branches (Table 2). Taking into account that the resins have similar weight comonomer content, different molar comonomer amounts correspond to each LLDPE samples, as reported in Table 1. Therefore, the resin LLDPE/butene has more numerous and shorter branches along the polymer backbone compared with the LLDPE/hexene and LLDPE/octene copolymers. It is reasonable to suppose that these latter are characterized by a linear molecular structure for wider regions along the polymer chains, and this may result in a higher density of entanglements respect to the LLDPE/butene resin and, consequently, in a delayed onset of sharkskin failure [16]. However, in order to support this hypothesis further experimental analyses have to be conducted to evidence how the entanglement density changes with comonomer size.

Only two (LLDPE/butene and mLLDPE/hexene) of the four resins investigated in this study experienced SSF at shear stress in the range 0.42–0.44 MPa. In this flow regime, the mechanism by which the slip of the polymer melt takes place has been extensively investigated in literature. Although SSF is often associated with adhesive failure at the melt/die interface [34–36], a recent molecular theory [8, 37] suggests that slip may be due to failure within the polymer but very close to the die wall (cohesive failure). In other words, the critical condition for the stick-slip discontinuity in polyethylenes occurs through a chain-chain entanglement/disentanglement process arising from a coil-stretch transition [38], i.e. the stretched chains at the die wall no longer entangle with the near-surface molecules. The flow stability analysis, conducted in this study on LLDPE/α-olefin copolymers, shows that, even increasing of few carbon atoms the SCB length of the resins, the stick-slip phenomenon is reduced and/or eliminated. In fact, among the conventional LLDPEs analyzed only the LLDPE/butene sample exhibits the stick-slip fracture. However, comparing the linear polyethylenes with the same comonomer type (hexene), the metallocene LLDPE also manifested the stick-slip regime above a critical wall shear stress ($\tau_w = 0.44$ MPa). The narrower MWD, which characterize this resin respect to its Ziegler-Natta counterpart, is responsible of the occurrence of the spurt flow for the metallocene polymer melt.

Finally, GMF was observed for all the materials investigated at critical shear stress in the range 0.49–0.55 MPa. It is worthy to point out that for all the conventional LLDPE copolymers analyzed this flow instability occurs at similar shear rates equal to about 2800 s^{-1}, while the metallocene linear polyethylene exhibits an earlier onset of GMF ($\dot{\gamma}_a = 1700 s^{-1}$). These results agree with those previously reported by other authors [9] on the delayed onset of GMF by broadening the MWD of polyethylenes. To our knowledge, no other reports exist in the literature regarding the effect of SCB length on GMF phenomenon of LLDPE resins. Although the flow pattern in GMF regime is believed to closely resemble the stick-slip mechanism [10], the increase of the SCB length in the Ziegler-Natta polyethylenes investigated in this work does not influence the occurrence of gross fracture. This result may be attributed to a fundamental difference between the stick-slip and gross flow regimes: the first occurs only close to the polymer-wall interface, while the second occurs at multiple polymer surfaces within the bulk of the material [10].

TABLE 2. Critical shear rates and stresses for all the resins in capillary die extrusion at 150°C.

Resin	Melt fracture type	$\dot{\gamma}_a$ (s^{-1})	τ_w (MPa)
LLDPE/butene	SHARKSKIN	130	0.20
	STICK-SLIP	920	0.42
	GROSS MELT	2600	0.52
LLDPE/hexene	SHARKSKIN	250	0.23
	GROSS MELT	2800	0.52
mLLDPE/hexene	SHARKSKIN	190	0.30
	STICK-SLIP	500	0.44
	GROSS MELT	1700	0.49
LLDPE/octene	SHARKSKIN	500	0.34
	GROSS MELT	2800	0.55

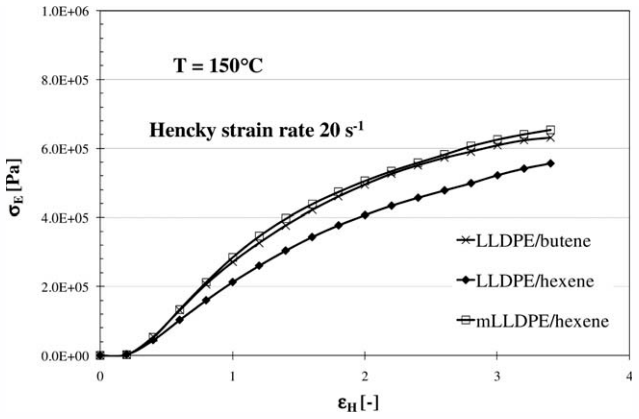

FIG. 12. Plot of the tensile stress as function of Hencky strain for the LLDPE/butene, LLDPE/hexene and mLLDPE/hexene, at a Hencky strain rate of 20 s^{-1} and at temperature of 150°C.

Effect of Processing Temperature

A basic strategy to eliminate or postpone flow instabilities in polymers is to rise the die temperature. In fact, it is well known that an increase in extrusion temperature corresponds to an attenuation of stress intensity, at the same strain rate, resulting in the reduction of the polymer "pre-stretching" condition, responsible for an easier appearance of melt fracture.

For all the LLDPE copolymers analyzed in this work an increase of the extrusion temperature shifted the onset of melt fracture to higher shear rates, while the critical shear stresses for the occurrence of sharkskin were almost independent on melt temperature (data shown in Table 3), as already reported in literature for other kinds of polyethylenes [39]. Moreover, the evolution of the flow instability for the resins was studied keeping constant the shear rate while varying the extrusion temperature. In particular, the comparison between the images of LLDPE/butene and LLDPE/octene extrudates, obtained at an apparent shear rate of 950 s^{-1} and different extrusion temperatures, is reported in Fig. 13. At this strain rate, typical of polymer processing operations, the melt fracture behavior of the conventional LLDPE copolymers showed comparable sensitivity to a temperature increment, irrespective of the different comonomer type used in polymerization, as also confirmed by the corresponding activation energies of the resins (Table 1). The temperature dependence of flow instability for the metallocene and conventional LLDPE samples, with the same comonomer (hexene), is shown in Fig. 14. The mLLDPE/hexene resin exhibited a more significant improvement in processing behavior, by increasing the extrusion temperature, compared with the LLDPE/hexene copolymer, in agreement with its slightly higher activation energy (Table 1).

TABLE 3. Critical shear rates and stresses corresponding to the onset of sharkskin for all the resins in capillary die extrusion at 150°C and 220°C.

Resin	Extrusion temperature (°C)	Onset SHARSKIN	
		$\dot{\gamma}_a$ (s^{-1})	τ_w (MPa)
LLDPE/butene	150	130	0.20
	220	600	0.22
LLDPE/hexene	150	250	0.23
	220	950	0.30
mLLDPE/hexene	150	190	0.30
	220	900	0.34
LLDPE/octene	150	500	0.34
	220	2500	0.38

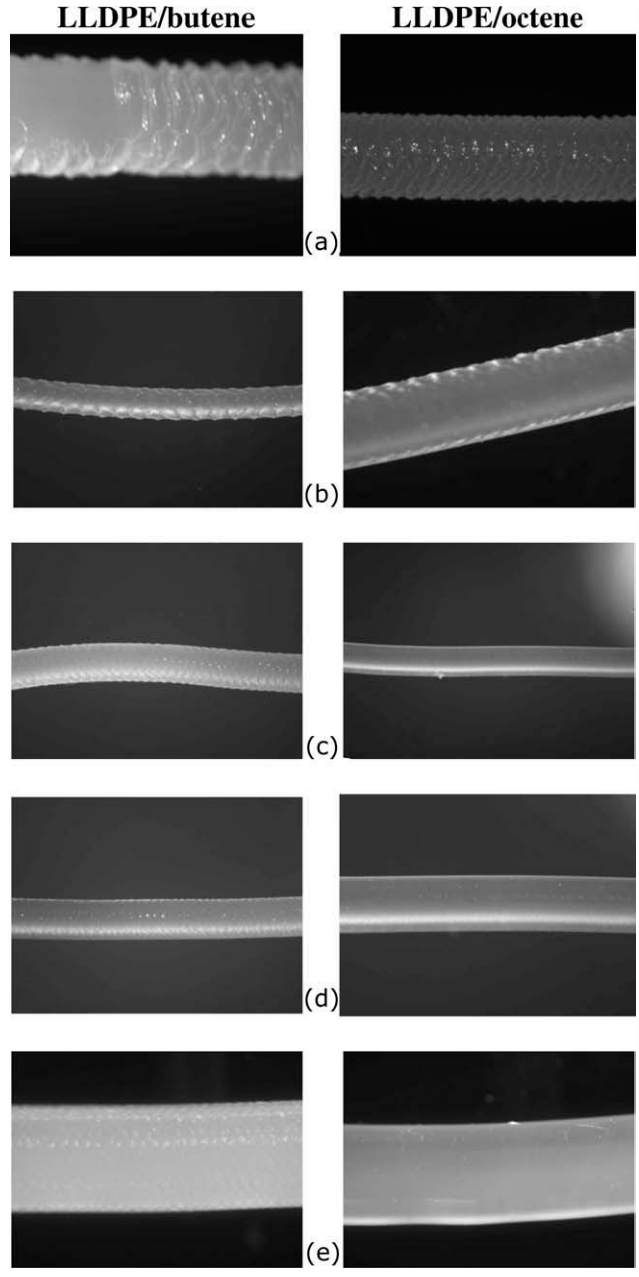

FIG. 13. Comparison between the images of LLDPE/butene and LLDPE/octene extrudates obtained at an apparent shear rate of 950 s^{-1} and different extrusion temperatures: (a) T = 150°C; (b) T = 190°C; (c) T = 200°C; (d) T = 210°C; (e) T = 220°C.

DOI 10.1002/pen

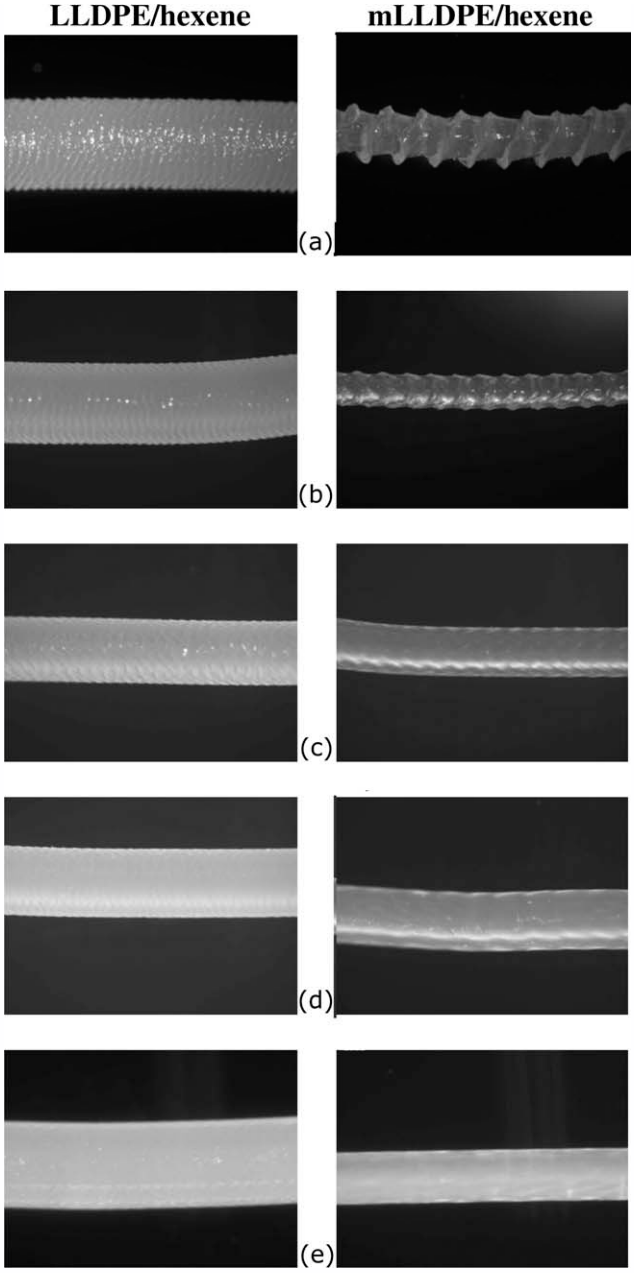

FIG. 14. Comparison between the images of LLDPE/hexene and mLLDPE/hexene extrudates obtained at an apparent shear rate of 950 s^{-1} and different extrusion temperatures: (a) T = 150°C; (b) T = 190°C; (c) T = 200°C; (d) T = 210°C; (e) T = 220°C.

CONCLUSIONS

The aim of this work was to analyze the effects that MWD and SCB length have on the observed melt fracture phenomena for poly(ethylene/α-olefin) resins with similar weight comonomer content and molecular weight. Further, the influence of the extrusion temperature on melt fracture behavior has also been analyzed.

The flow stability analysis conducted in this study has shown that, even increasing of few carbon atoms the SCB length of the resins, the SMF phenomena (SMF and SSF) are reduced and/or eliminated. On the contrary, the occurrence of GMF, in the Ziegler-Natta polyethylenes, was not influenced by the type of α-olefin used as comonomer. Moreover, for all the conventional LLDPE resins an increase of the extrusion temperature shifted the onset of melt fracture to higher shear rates.

Comparing the metallocene and the conventional LLDPE samples, polymerized using the same comonomer (hexene), the metallocene resin exhibited early onset and more severe melt fracture, due to its narrower MWD. On the other hand, compared with its conventional counterpart, the mLLDPE/hexene resin showed a more significant improvement in processing behavior by increasing the extrusion temperature, in agreement with its higher activation energy,.

REFERENCES

1. P.J. Doerpinghaus and D.G. Baird, *Rheol. Acta.*, **42**, 544 (2003).
2. J.M. Piau, N. El Kissi, F. Toussaint, and A. Mezghani, *Rheol. Acta.*, **34**, 40 (1995).
3. E.R Howells and J.J. Benbow, *Trans. J. Plast. Inst.*, **30**, 240 (1962).
4. F.N. Cogswell, *J. Non-Newton. Fluid.*, **2**, 37 (1977).
5. A.V. Ramamurthy, *J. Rheol.*, **30**, 337 (1986).
6. D.S. Kalika and M.M. Denn, *J. Rheol.*, **31**, 815 (1987).
7. V.G. Ghanta, B.L. Riise, and M. Denn., *J. Rheol.*, **43**, 435 (1999).
8. F. Brochard and P.G. de Gennes, *Langmuir.*, **8**, 3033 (1992).
9. S. Kim and J.M. Dealy, *Polym. Eng. Sci.*, **42**, 495 (2002).
10. M. Sentmanat, and S.G. Hatzikiriakos, *Rheol. Acta.*, **43**, 624 (2004).
11. E.B. Muliawan, S.G. Hatzikiriakos, and M. Sentmanat, *Int. Polym. Proc.*, **XX**, 60 (2005).
12. J.P. Tordella, *Unstable Flow of Molten Polymers. Rheology: Theory and Applications*, Accademic Press, New York (1969).
13. S. His-Hsin, C. Min Wong, Y. Wang, C. Huang, and C.C. Wu, *J. Appl. Polym. Sci.*, **73**, 1769 (1999).
14. L.C.P. Shan, J.B.P. Soares, and A. Penlidis, *Polymer.*, **43**, 767 (2002).
15. R.A. Bubeck, *Mater. Sci. Eng.*, **39**, 1 (2002).
16. M. Yamaguchi, H. Miyata, V. Tan, and C.G. Gogos, *Polymer.*, **43**, 5249 (2002).
17. Z. Tao and J.C. Huang, *J. Appl. Polym. Sci.*, **98**, 903 (2005).
18. F.J. Stadler, C. Gabriel, and H. Münstedt, *Macromol. Chem. Physic.*, **208**, 2449 (2007).
19. M. Sentmanat, *Rheol. Acta.*, **43**, 657 (2004).
20. M. Sentmanat, B.N. Wang, and G.H. McKinley, *J. Rheol.*, **49**, 585 (2005).
21. V.R. Raju, G.G. Smith, G. Marin, J.R. Knox, and W.W. Graessley, *J. Polym. Sci. Pol. Phys.*, **17**, 1183 (1979).
22. J.F. Vega, A. Santamaria, A. Munoz-Escalona, and P. Lafuente, *Macromolecules.*, **31**, 3639 (1998).

23. J. L. White and H. Yamane, *Pure. Appl. Chem.*, **59**, 193 (1987).
24. H. Mavridis and R. Shroff, *J. Appl. Polym. Sci.*, **49**, 299 (1993).
25. J.F. Vega, M. Ferna'ndez, A. Santamaria, A. Munoz-Escalona, and P. Lafuente, *Macromol. Chem. Physic.*, **200**, 2257 (1999).
26. P.J. Doerpinghaus and D.G. Baird, *J. Rheol.*, **47**(3), 717 ,(2003).
27. S.G. Hatzikiriakos, *Polym. Eng. Sci.*, **40**, 2279 (2000).
28. K.W. Swogger, G.M. Lancaster, S.Y. Lai, and T.I. Butler, *J. Plast. Film. Sheet.*, **11**, 102 (1995).
29. H. Mavridis, and R.N. Shroff, *Polym. Eng. Sci.*, **32**, 1778 (1992).
30. D. Bonchev, A.H. Dekmezian, E. Markel, and A. Faldi, *J. Appl. Polym. Sci.*, **90**, 2648 (2003).
31. E.E. Rosenbaum, S.G. Hatzikiriakos, and C.W. Stewart, *Int. Polym. Proc.*, **X**, 204 (1995).
32. M. Sentmanat, E.B. Muliawan, and S.G. Hatzikiriakos, *Rheol. Acta.*, **44**, 1 (2004).
33. H.H. Kausch, *Polymer Fracture*, Chapter 9, Springer, Berlin (1978).
34. D.A. Hill, T. Hasegawa, and M.M. Denn, *J. Rheol.*, **34**, 891 (1990).
35. S.G. Hatzikiriakos, *Int. Polym. Proc.*, **8**, 135 (1993).
36. S.H. Anastasiadis and S.G. Hatzikiriakos, *J. Rheol.*, **42**, 795 (1998).
37. X. Yang, S.Q. Wang, and A. Halasa, *Rheol. Acta.*, **37**, 415 (1998).
38. S.Q. Wang and P.A. Drda, *Macromolecules.*, **29**, 4115 (1996).
39. M. Aguilar, J.F. Vega, A. Muňoz-Escalona, and J. Martínez-Salazar, *J. Mater. Sci.*, **37**, 3415 (2002).

 DOI 10.1002/pen